Defective DNA repair and increased genomic instability in Cernunnos-XLF-deficient murine ES cells

Shan Zha, Frederick W. Alt*, Hwei-Ling Cheng, James W. Brush, and Gang Li

Howard Hughes Medical Institute, Children's Hospital, CBR Institute for Biomedical Research, Harvard Medical School, Boston, MA 02115

Contributed by Frederick W. Alt, January 4, 2007 (sent for review December 28, 2006)

Nonhomologous DNA end-joining (NHEJ) is a major pathway of DNA double-strand break (DSB) repair in mammalian cells, and it functions to join both specifically programmed DSBs that occur in the context of V(D)J recombination during early lymphocyte development as well as general DSBs that occur in all cells. Thus, defects in NHEJ impair V(D)J recombination and lead to general genomic instability. In human patients, mutations of Cernunnos-XLF (also called NHEJ1), a recently identified NHEJ factor, underlie certain severe combined immune deficiencies associated with defective V(D)J recombination and radiosensitivity. To characterize Cernunnos-XLF function in mouse cells, we used gene-targeted mutation to delete exons 4 and 5 from both copies of the *Cernunnos-XLF* gene in ES cell (referred to as $Cer^{\Delta/\Delta}$ ES cells). Analyses of $Cer^{\Delta/\Delta}$ ES cells showed that they produce no readily detectable Cernunnos-XLF protein. Based on transient V(D)J recombination assays, we find that $Cer^{\Delta/\Delta}$ ES cells have dramatic impairments in ability to form both V(D)J coding joins and joins of their flanking recombination signal sequences (RS joins). $Cer^{\Delta/\Delta}$ ES cells are highly sensitive to ionizing radiation and have intrinsic DNA DSB repair defects as measured by pulse field gel electrophoresis. Finally, the *Cernunnos-XLF* mutations led to increased spontaneous genomic instability, including translocations. We conclude that, in mice, Cernunnos-XLF is essential for normal NHEJ-mediated repair of DNA DSBs and that Cernunnos-XLF acts as a genomic caretaker to prevent genomic instability.

nonhomologous DNA end-joining | severe combined immunodeficiency | V(D)J recombination

DNA double-strand breaks (DSBs) can result from a variety of factors, including ionizing radiation (IR), oxidative damage, replication errors, and genetically programmed processes such as V(D)J recombination in developing lymphocytes. As the consequences of unrepaired or misrepaired DSBs range from cell death to genomic instability and oncogenic transformation, cells have efficient systems to detect and repair DNA DSBs. In mammalian cells, there are two major DNA DSB repair pathways, homologous recombination that promotes repair by using the intact copy of homologous sequence as template in postreplication cell cycle phases and nonhomologous DNA end-joining (NHEJ) that joins broken DNA ends independent of homology (1, 2). The NHEJ pathway contains six well characterized members. Four "core" NHEJ components are clearly conserved in evolution and include the Ku70 and Ku80 proteins that function as a DNA end-binding complex and XRCC4 and DNA Ligase 4 (Lig4) proteins that function as a complex in end-ligation (1, 3). These proteins are required for all known NHEJ reactions. Two other members, DNA-dependent kinase catalytic subunit (DNA-PKcs) and Artemis, appear to have arisen more recently in evolution, and their functions are required, at least in part, for joining those ends that need processing before joining (3). In this context, after DNA-PKcs bind to DNA ends, through interaction with Ku, it can activate an endonuclease function in Artemis (4).

During early lymphocyte development, the exons that encode the variable regions of Ig and T cell receptor genes are assembled from germ-line V, D, and J segments through the process of V(D)J recombination (3). V(D)J recombination is initiated by the RAG endonuclease, which introduces DNA DSBs between the participating V, D, or J coding sequences and their flanking recombination signal sequences (RS). The RAG cleavage reaction generates two distinct intermediates: blunt 5′ phosphorylated RS ends and the covalently sealed hairpin-coding ends (3). Two coding ends or two RS ends are then joined, respectively, to form V(D)J coding and RS joins by NHEJ (3). Ku70, Ku80, XRCC4, and Lig4 are required for the generation of both coding and RS joins. On the other hand, DNA-PKcs and Artemis are required primarily for coding end joining, where the Artemis endonuclease activity is necessary to open and process coding end hairpins (3, 4). Hairpin opening at points other than the apex results in overhanging nucleotides that lead to the addition of short (1–2 bp) palindromic nucleotides (P-elements). Furthermore *N*-nucleotide addition by terminal deoxynucleotidyl transferase (TdT) also contributes to the junctional diversification of coding joins (3). Finally, XRCC4 and Lig4 work together to complete both coding and RS joins (3).

There are murine models for deficiencies of all known NHEJ factors except the newly identified Cernunnos-XLF factor (see below). Deficiencies for Ku70, Ku80, XRCC4, and Lig4 lead to cellular IR sensitivity, growth defects, and increased genomic instability (1, 3). Deficiency for any of these four factors leads to a severe combined immune deficiency (SCID) phenotype, because of inability to generate V(D)J joins, and to severe apoptosis of newly generated neurons (1, 3). XRCC4 and Lig4 deficiency also cause late embryonic lethality, perhaps because the neuronal apoptosis is so severe (3). Deficiency for DNA-PKcs and Artemis also leads to a SCID phenotype, because of the defect in generating V(D)J coding joins, but do not lead to growth defects or increased neuronal apoptosis (1, 3). DNA-PKcs and Artemis-deficient cells have variable IR sensitivity. Consistent with cellular genomic instability, mice deficient for any of the six known NHEJ factors in a p53-deficient background inevitably succumb to pro-B cell lymphomas harboring RAG-dependent oncogenic IgH locus translocations (1, 3).

Cernunnos-XLF is the most recently identified factor required for NHEJ (5–7). Several inherited mutations of *Cernunnos-XLF* have been identified in human patients. Recently, a balanced translocation that interrupts Cernunnos-XLF gene, has been identified in a fetal autopsy sample and suggested to be associated with polymicrogyria (8). Although well characterized human mutations range from severe truncations to point mutations, all result in very

Author contributions: S.Z. and G.L. contributed equally to this work; S.Z., G.L., and F.W.A. designed research; S.Z., J.W.B., H.-L.C., and G.L. performed research; S.Z., J.W.B., H.-L.C., and G.L. analyzed data; and S.Z. and F.W.A. wrote the paper.

The authors declare no conflict of interest.

Abbreviations: DSB, double strand break; IR, ionizing radiation; NHEJ, nonhomologous DNA end-joining; RS, recombination signal sequence; SCID, severe combined immune deficiency.

*To whom correspondence should be addressed. E-mail: alt@enders.tch.harvard.edu.

This article contains supporting information online at www.pnas.org/cgi/content/full/0611734104/DC1.

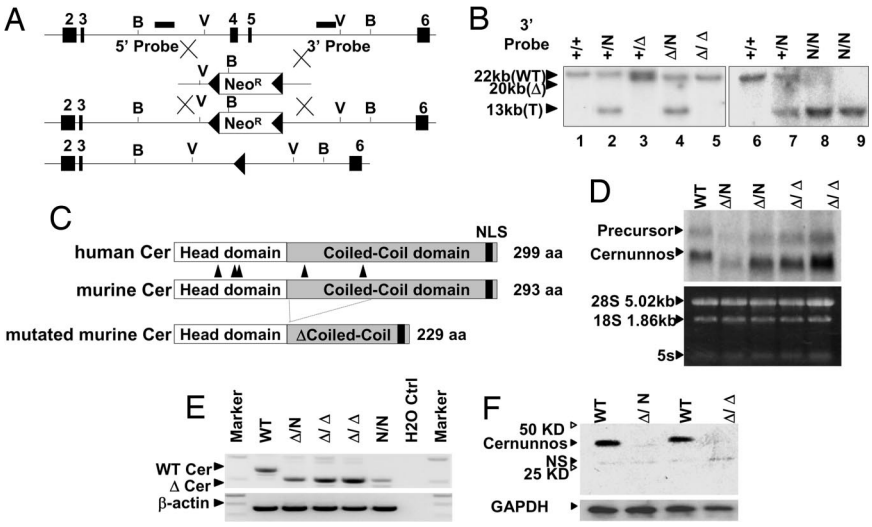

Fig. 1. Gene-targeted deletion of Cernunnos-XLF in murine ES cells. (*A*) The schematic diagram represents murine Cernunnos-XLF locus (*Top*), targeting vector (*Second Row*), targeted allele (Cer^{N}, *Third Row*), and the deleted allele (Cer^{Δ}, *Bottom*). The 3′ and 5′ probes are marked as black lines. The exons and loxP sites are shown as filled boxes and filled triangles respectively. Restriction site designation: B, BamHI; V, EcoRV. The map is not drawn to scale. (*B*) Southern blot analysis of BamHI-digested DNA from WT (lane 1), $Cer^{+/N}$(lane 2), $Cer^{+/\Delta}$ (lane 3), $Cer^{\Delta/N}$ (lane 4), and $Cer^{\Delta/\Delta}$ (lane 5) ES cells. Lanes 6–9 represent the parent WT TC1 ES cells (lane 6), intermediate targeting (lane 7), and the homozygous Cernunnos-XLF-deficient ES cells (lanes 8 and 9) obtained through high-G418 selection and Cre deletion. The location of the 3′ probe is indicated in *A*. (*C*) Schematic representation of the human Cernunnos-XLF protein and the predicted truncated protein from $Cer^{\Delta/\Delta}$ ES cells. Black triangles indicate the position of Cernunnos-XLF mutations identified in six human patients (two patients contain the same mutation) (5, 6). (*D*) Northern blot analysis of total RNA (20 μg) from WT and four different Cernunnos-XLF-deficient ES cells probed with the ORF of mouse *Cernunnos-XLF*. (*E*) RT-PCR analysis with primers flanking the entire ORF of the murine *Cernunnos-XLF* gene from WT or Cernunnos-XLF-deficient ES cells. (*F*) Western blot analyses of total protein (50 μg) from WT, $Cer^{N/\Delta}$, and $Cer^{\Delta/\Delta}$ ES cells. The predicted size for authentic Cernunnos-XLF and a faint nonspecific (NS) band are indicated with filled arrowheads.

similar clinical presentations (5–7), including growth retardation, microcephaly, and SCID that generally appears less severe than that associated with inactivating mutations of Artemis (9). However, the SCID phenotype of Cernunnos-XLF patients tends to get progressively worse with age (5–7). Fibroblasts derived from Cernunnos-XLF-mutated patients show severe defects in ability to generate either coding or RS joins in the context of extrachromosomal V(D)J recombination substrate assays and display hypersensitivity to IR and other DSB-inducing agents (5–7), indicative of a DNA DSB repair defect. In addition, Cernunnos-XLF forms a complex with Lig4 and XRCC4 *in vitro* and has been predicted, in structure simulation analyses, to share features with XRCC4, including an N-terminal head domain and a C-terminal coiled-coil domain (5, 10, 11). Moreover, Cernunnos-XLF appears to have a homolog in yeast, termed Nej1 (10–15), which interacts with Lif1p, which appears to be the yeast XRCC4 homolog (16), suggesting that Cernunnos-XLF may represent a "core" NHEJ factor. To further elucidate the function of Cernunnos-XLF in V(D)J recombination, DNA repair, and genomic stability in mice, we report the generation and characterization of Cernunnos-XLF-deficient murine ES cells.

Results

Generation of Cernunnos-XLF-Mutant ES Cell Lines. We targeted a neomycin-resistant cassette (Neo^{R}) in place of exons 4 and 5 of *Cernunnos-XLF* in TC1 ES cells (Fig. 1*A*). Correctly targeted TC1 clones ($Cer^{+/N}$) were identified by the appearance of a unique 13-kb band as determined by Southern blotting of BamHI-digested genomic DNA with a genomic probe that lies 3′ of the mutated region of the *Cernunnos-XLF* gene (Fig. 1 *A* and *B*). $Cer^{+/N}$ ES cells were infected with adenovirus expressing Cre recombinase (Adeno-Cre) to remove the Neo^{R} cassette and generate $Cer^{+/\Delta}$ ES cells; the Neo-deleted allele was identified as a 20-kb BamHI fragment that hybridized to the 3′ probe (Fig. 1*B*). $Cer^{+/\Delta}$ ES cells were subjected to a second round of targeting to generate $Cer^{\Delta/N}$ ES cells. With the 3′ probe, successful targeting of the second allele was identified based on complete loss of a 22-kb germ-line Cernunnos-XLF band, retention of a 20-kb fragment represented the Neo^{R}-deleted allele (Cer^{Δ}), and appearance of a 13-kb targeted band containing the Neo^{R} cassette (Cer^{N}) (Fig. 1*B*). Finally, $Cer^{\Delta/N}$ clones were exposed to Adeno-Cre virus to obtain ES cells that were homozygous for the exon 4/5 deletion ($Cer^{\Delta/\Delta}$) and that were identified as containing only the 20-kb band (Fig. 1*B*). We also

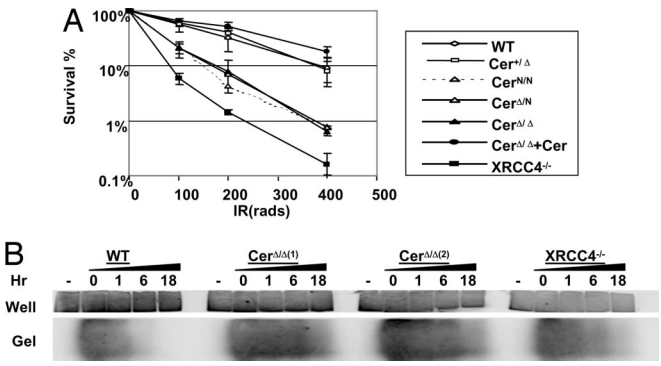

Fig. 2. Increased IR sensitivity and DNA double-strand-break repair defects of Cernunnos-XLF mutant ES cells. (*A*) IR sensitivity of WT (TC1), $XRCC4^{-/-}$, $Cer^{+/\Delta}$, $Cer^{N//N}$, $Cer^{N/\Delta}$, $Cer^{\Delta/\Delta}$, and $Cer^{\Delta/\Delta}$ ES cells that express the WT Cernunnos-XLF cDNA from a PGK promoter ($Cer^{\Delta/\Delta}$ + Cer). The percentage of surviving colonies in comparison to unirradiated cells is plotted as the function of irradiation dose (rad). Each data point represents the average of at least two (most times three) independent experiments performed on at least two independent ES cell clones. (B) Cernunnos-XLF deficiency causes DNA DSB repair defects. Sybr green-stained pulse-field gel electrophoresis analysis of DNA from WT (TC1), $XRCC4^{-/-}$, and two independent clones of $Cer^{\Delta/\Delta}$ ES cells at various times after exposure to 80Gy γ-irradiation. The level of repair is inversely correlated with the amount of DNA in the gel at a given time point versus the amount of DNA that enters the gel immediately after radiation (0 h time point). See *Materials and Methods* and *Results* for other details of the assay.

Table 1. Analysis of coding joins in Cernunnos-XLF deficient ES cells

	Cell line	(Amp^r+Cam^r)/Amp^r	Percentage	Relative level
Exp1	WT	62/6,300	0.9887	
	$Cer^{\Delta/\Delta(1)}$	2/37,000	0.0060	0.0060
	$XRCC4^{-/-}$	10/339,000	0.0029	0.0030
Exp2	WT	82/9,200	0.8913	
	$Cer^{\Delta/\Delta(1)}$	7/67,000	0.0104	0.0117
	$Cer^{\Delta/\Delta(2)}$	4/45,000	0.0089	0.0100
	$XRCC4^{-/-}$	8/149,000	0.0054	0.0061
Exp3	WT	99/21,000	0.4709	
	$Cer^{\Delta/\Delta(1)}$	2/72,000	0.0031	0.0065
	$XRCC4^{-/-}$	0/80,000	<0.0013	<0.0027
Exp4	WT	432/148,800	0.2903	
	$Cer^{N/N(1)}$	36/232,000	0.0155	0.0533
	$Cer^{N/N(2)}$	19/140,800	0.0135	0.0464
	$XRCC4^{-/-}$	0/64,600	<0.0015	<0.0004
Exp5	WT	303/35,000	0.8657	
	$Cer^{N/N(1)}$	58/88,800	0.0653	0.0754
	$Cer^{N/N(2)}$	51/144,000	0.0354	0.0409
	$XRCC4^{-/-}$	2/15,800	0.0013	0.0015
Exp6	WT	145/147,200	0.0985	
	$Cer^{\Delta/\Delta(1)}$	11/235,200	0.0047	0.0474
	$Cer^{N/N(1)}$	1/27,800	0.0036	0.0365
	$Cer^{N/N(2)}$	3/52,800	0.0057	0.0576
	$XRCC4^{-/-}$	0/22,800	<0.0044	<0.0445
Exp7	WT	820/120,000	0.6833	
	$Cer^{\Delta/\Delta}$	34/324,000	0.0105	0.0154
	$Cer^{\Delta/\Delta}$+Cer(1)	792/200,000	0.3960	0.5795
	$Cer^{\Delta/\Delta}$+Cer(2)	720/142,000	0.5070	0.7420
	$XRCC4^{-/-}$	0/70,000	<0.0014	<0.0021
	No RAG	0/148,000	<0.0007	<0.0010

Table 2. Analysis of RS joins in Cernunnos-XLF-deficient ES cells

	Cell line	(Amp^r+Cam^r)/Amp^r	Percentage	Relative level
Exp1	WT	110/12,000	0.9167	
	$Cer^{\Delta/N}$	1/35,000	0.0029	0.0031
	$Cer^{\Delta/\Delta(2)}$	17/119,000	0.0143	0.0155
	$XRCC4^{-/-}$	0/37,000	<0.0027	<0.0029
Exp2	WT	41/4,800	0.8542	
	$Cer^{\Delta/\Delta(1)}$	6/65,000	0.0092	0.0108
	$Cer^{\Delta/\Delta(2)}$	4/73,000	0.0055	0.0064
	$XRCC4^{-/-}$	1/82,000	0.0012	0.0014
Exp3	WT	210/22,000	0.9545	
	$Cer^{N/N(1)}$	24/132,000	0.0185	0.0194
	$XRCC4^{-/-}$	1/82,000	0.0012	0.0014
Exp4	WT	119/38,600	0.3083	
	$Cer^{N/N(1)}$	2/28,600	0.0070	0.0227
	$Cer^{N/N(2)}$	3/55,600	0.0054	0.0175
	$XRCC4^{-/-}$	0/16,800	<0.0060	<0.0193
Exp5	WT	23/15,600	0.1474	
	$Cer^{\Delta/\Delta(3)}$	1/18,800	0.0053	0.0361
	$Cer^{\Delta/\Delta(4)}$	1/35,800	0.0028	0.0189
	$Cer^{N/N(1)}$	4/131,200	0.0030	0.0207
	$XRCC4^{-/-}$	0/15,400	<0.0065	<0.0441
Exp5	WT	84/22,000	0.3818	
	$Cer^{\Delta/\Delta}$	72/314,000	0.0229	0.0601
	$Cer^{\Delta/\Delta}$+Cer(1)	936/188,000	0.4979	1.3040
	$Cer^{\Delta/\Delta}$+Cer(2)	760/177,500	0.4282	1.1214
	$XRCC4^{-/-}$	1/75,000	0.0013	0.0035
	No RAG	0/66,500	<0.0015	<0.0039

exposed $Cer^{+/N}$ cells to increased levels of G418 to obtain homozygous Cernunnos-XLF targeted ES cells ($Cer^{N/N}$), which were identified by disappearance of a 22-kb germ-line band with retention of only the 13-kb Neo^R-targeted band. A 5′ probe was used to confirm all clones [supporting information (SI) Fig. 4*A* and data not shown]. Four independent $Cer^{\Delta/\Delta}$ or $Cer^{N/N}$ clones were subcloned and used for subsequent analyses.

Our targeting strategy should lead to an in-frame splicing from exon 3 to exon 6 of the *Cernunnos-XLF* gene and production of a transcript that is 198-bp smaller than the WT transcript. Northern blot and RT-PCR analyses confirmed that $Cer^{\Delta/\Delta}$ ES cells made the predicted truncated transcript (Fig. 1 *D* and *E*). This transcript potentially could be translated into a truncated protein that lacks a large portion of the coiled-coil domain (Fig. 1*C*), a predicted protein interaction domain (5, 10), and as such may well be nonfunctional in any case. To confirm that authentic Cernunnos-XLF was not made in $Cer^{\Delta/\Delta}$ ES cells, we used an antibody that recognizes the C-terminal region of Cernunnos-XLF to perform Western blot analysis on extracts from WT (TC1) and $Cer^{\Delta/\Delta}$ ES cells. Although we readily detected the authentic 37kD Cernunnos-XLF protein in extracts from WT TC1 cells, we failed to detect any obvious Cernunnos-XLF cross-reacting proteins from multiple $Cer^{\Delta/\Delta}$ and $Cer^{\Delta/N}$ ES cells lines (Fig. 1*F*). However, given that there was a very low level of a cross-reacting band in WT cells (smaller in size than the predicted band from the mutant Cernunnos-XLF transcript) that migrates below the authentic Cernunnos-XLF band (Fig. 1*F*), we cannot absolutely rule out the presence of very small amounts of an unexpected Cernunnos-XLF translation product in $Cer^{\Delta/\Delta}$ ES cells.

Cernunnos-XLF Mutant ES Cells Are Sensitive to Ionizing Radiation and Have DSB Repair Defects. To determine the effect of the homozygous Cernunnos-XLF mutation on IR sensitivity, we used a colony-survival assay to compare radiosensitivity of WT (TC1), $Cer^{\Delta/\Delta}$, $Cer^{N/N}$, and $XRCCR4^{-/-}$ ES cells. In multiple experiments conducted with independent ES clones, $Cer^{\Delta/\Delta}$ and $Cer^{N/N}$ ES cells consistently showed markedly increased sensitivity to IR as compared with WT ES cells. Radiosensitivity of the Cernunnos-XLF mutant ES cells approached that of XRCC4-deficient ES cells, which are very highly IR-sensitive (Fig. 2*A*). Notably, $Cer^{+/\Delta}$ ES cells do not have any significant increase of IR sensitivity when compared with the WT ES cells, indicating no substantial haploinsufficient phenotype and also suggesting that the Cer^{Δ} allele does not generate a dominant-negative phenotype (Fig. 2*A*). Finally, introduction of full-length Cernunnos-XLF protein expressed from a vector stably transfected into $Cer^{\Delta/\Delta}$ ES cells restored the IR sensitivity back to WT levels (Fig. 2*A*; SI Fig. 4*B*), demonstrating that Cernunnos-XLF deficiency is specifically responsible for the increased IR sensitivity of $Cer^{\Delta/\Delta}$ ES cells.

To determine whether the IR-sensitivity of $Cer^{\Delta/\Delta}$ ES cells is associated with an intrinsic defect in DNA DSB repair, we measured the level of DNA fragmentation at different time points after irradiation (80 Gy) in WT (TC1), $Cer^{\Delta/\Delta}$, and $XRCCR4^{-/-}$ ES cells by pulse-field gel electrophoresis (Fig. 2*B*) (17, 18). Immediately after irradiation, a significant amount of genomic DNA from all cells ran out of the wells and into the gel, indicating massive DNA fragmentation. By 6 h after irradiation, the majority of genomic DNA from WT cells was retained in the well, indicative of efficient DNA DSB repair (Fig. 2*B*). However, in $Cer^{\Delta/\Delta}$ and $XRCCR4^{-/-}$ ES cells, a significant amount of genomic DNA ran into the gel even 18 h after the irradiation, indicating defective ability to repair DNA DSBs (Fig. 2*B*). Therefore, as measured by this crude assay, $Cer^{\Delta/\Delta}$ ES cells, like $XRCC4^{-/-}$ ES cells, have a significant DSB repair defect (Fig. 2*B*).

Cernunnos-XLF Is Required for Efficient V(D)J Recombination of Both Coding and RS Joins in ES Cells. To evaluate the role of Cernunnos-XLF in V(D)J recombination in murine cells, we used a transient V(D)J recombination assay (19–21). WT (TC1) and $Cer^{\Delta/\Delta}$ ES cells plus $XRCC4^{-/-}$ ES cells (which cannot form either coding or RS joins) were transfected with vectors that express full-length RAG1 and RAG2 proteins and a plasmid recombination substrate that is designed to measure the frequency of either coding (pJH290) or RS (pJH200) joining. A transcriptional terminator lying between two

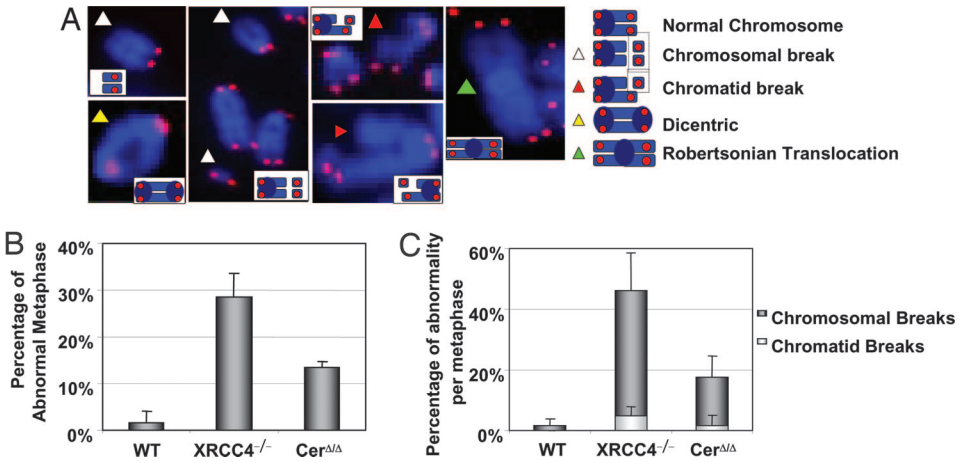

Fig. 3. Spontaneous genomic instability in Cernunnos-XLF-deficient ES cells. (*A*) Examples of cytogenetic abnormalities observed in untreated Cernunnos-XLF-deficient ES cell. DAPI-stained chromosomes are blue, with the centromeres being visualized as more intense blue ovals. Orange/red dots come from telomere signals. Color-coded arrowheads and corresponding cartoons indicate the different kinds of cytogenetic abnormalities that were scored (white, chromosomal break; red, chromatid break; yellow, dicentric chromosomes; green, Robertsonian translocation). One form of chromosomal break illustrated is a small piece of chromosome that contains telomeres and lacks centromeres; this anomaly is present in ≈50% of metaphases that have a chromosome that lacks telomeres on its long arms and likely represents two pieces of a broken chromosome as clearly illustrated in ref. 32. (*B*) Percentage of abnormal metaphases from WT, XRCC4$^{-/-}$, and Cernunnos-XLF-deficient ES cells quantified by telomere FISH (T-FISH) analyses. (*C*) Frequency of cytogenetic abnormality per metaphase in WT, XRCC4$^{-/-}$, and Cernunnos-XLF-deficient ES cells. The filled bars represent chromosomal breaks, and the open bars represent chromatid breaks. The data in *B* and *C* represents the average and standard deviation of three independent experiments from two independent WT ES cell lines, one XRCC4$^{-/-}$ line, and three independent Cer$^{\Delta/\Delta}$ or Cer$^{N/N}$ ES cell lines. We note certain limitations to the T-Fish assay, which generally could result in an underestimation of chromosome breaks and translocations, in *Materials and Methods*.

coding/RS sequences blocks expression of the chloramphenicol acetyl-transferase from the recombination substrate plasmid. Successful V(D)J recombination between two coding or RS ends allows the expression of the chloramphenicol acetyl-transferase. The relative efficiency of V(D)J recombination is determined by transforming plasmids recovered from the transfected cells into bacteria and quantifying the ratio of chloramphenicol–ampicillin double-resistant clones (recombined plasmids) versus ampicillin-resistant clones (total plasmids recovered) (22).

In comparison with WT (TC1) ES cells, Cernunnos-XLF-deficient ES cells showed dramatically reduced ability to support V(D)J recombination on either the coding or RS-joining substrates, with levels in most experiments being ≈2 orders of magnitude lower than those obtained with WT ES cells. However, for both coding and RS joins, it did appear that V(D)J recombination levels in Cernunnos-XLF mutant ES cells were, on average, above those of XRCC4$^{-/-}$ ES cells, which generally show only background levels (Tables 1 and 2). In this regard, coding joins that could be recovered from Cer$^{\Delta/\Delta}$ ES cells, in contrast to those from other NHEJ-deficient cells, appeared similar to those recovered from WT ES cells with respect to length and degree of junctional deletions and additions (SI Fig. 5 *A* and *B*). Likewise, ≈75% (24 of 32) of RS joins recovered from Cer$^{\Delta/\Delta}$ ES cells were precise as determined by ApaLI digestion and confirmed by nucleotide sequencing (SI Fig. 5*C*). To confirm that the coding and RS joining defects observed in Cer$^{\Delta/\Delta}$ ES cells were due to the mutation in *Cernunnos-XLF*, we assayed Cer$^{\Delta/\Delta}$ ES cells that expressed a full-length Cernunnos-XLF cDNA and found essentially WT levels of coding and RS join formation, indicating that the observed defects were specifically associated with mutation of the Cernunnos-XLF gene (Tables 1 and 2).

Table 3. Spontaneous genomic instability in Cernunnos-deficient ES cells

Cell line	Metaphase	Abnormal metaphase, *n* (%)	Abnormality, *n* (%)	S.Br/T.Br*	Classification
WT	40	0	0	0	
Cer$^{\Delta/\Delta}$	40	5 (12.5)	7 (17.5)	5/2	1 dicentric, 2 chromatid breaks†
XRCC4$^{-/-}$	40	10 (25)	14 (35)	13/1	2 Robertsonian translocations‡
WT	30	1 (3.3)	1 (3.3)	1/0	
Cer$^{N/N}$	29	5 (17.2)	7 (24.1)	7/0	2 Robertsonian translocations
Cer$^{N/N}$	28	3 (10.7)	3 (10.7)	3/0	1 dicentric, 1 Robertsonian translocation
XRCC4$^{-/-}$	28	9 (32.1)	16 (54.1)	14/2	1 chromatid fusion
WT	40	0	0	0	
Cer$^{\Delta/\Delta}$	40	6 (15.0)	6 (15.0)	5/1	1 dicentric, 1 Robertsonian translocation
Cer$^{\Delta/\Delta}$	40	7 (17.5)	8 (20.0)	7/1	1 Robertsonian translocation
XRCC4$^{-/-}$	40	9 (22.5)	12 (30.0)	10/2	2 Robertsonian translocations

*S.Br, chromosomal break; T.Br, chromatid break.

†Only clear chromatid breaks, as those shown in Fig. 3*A*, are scored. Some cytogenetic changes that are not clearly visible by T-FISH, such as gap, are not scored.

‡Only Robertsonian translocation and dicentric chromosomes are scored as translocation. Translocations that maintain the centromere and telomere orientation cannot be scored by T-FISH. Therefore, the actual frequency of translocations might be higher than estimated by T-FISH.

Cernunnos-XLF Mutant ES Cells Have Increased Levels of Genomic Instability. To determine potential roles of Cernunnos-XLF in maintenance of genomic stability, we used a FISH assay that combines DAPI staining with a telomere-specific PNA probe (T-FISH) to assay metaphase chromosomes in WT (TC1), $Cer^{\Delta/\Delta}$, $Cer^{N/N}$, and $XRCC4^{-/-}$ ES cells. Three independent Cernunnos-XLF mutant ES cells lines (two $Cer^{\Delta/\Delta}$ and one $Cer^{N/N}$) were analyzed, and all exhibited increased levels of chromosomal abnormalities relative to WT ES cells, including chromosomal breaks and translocations (Table 3 and Fig. 3 *A* and *B*). Although the level of genomic instability observed in Cernunnos-XLF mutant ES cells was, on average, about half that observed in $XRCC4^{-/-}$ ES cells, the overall pattern of chromosomal abnormalities revealed similarities. In both Cernunnos-XLF-mutant and XRCC4-deficient ES cells, the major cytogenetic abnormalities involved chromosomal breaks (27 of 31 for $Cer^{\Delta/\Delta}$ or $Cer^{N/N}$ and 37 of 42 for $XRCC4^{-/-}$), whereas chromatid breaks were more rare (4 of 31 for $Cer^{\Delta/\Delta}$ or $Cer^{N/N}$ and 5 of 42 for $XRCC4^{-/-}$) (Fig. 3*C* and Table 3). These results suggest that, like XRCC4 (23, 24), Cernunnos-XLF has a more major function in DSB repair in prereplicative cell cycle phases. In addition, as for XRCC4-deficient cells, a significant percentage of chromosomal breaks in Cernunnos-XLF-mutant ES cells participate in translocations (Fig. 3*A* and Table 3). Notably, we did not observe any telomere fusions in Cernunnos-XLF mutant ES cells as telomere signals were lost from both partner chromosomes in all observed translocations/fusions (Fig. 3 *A* and *B*). Overall, these findings demonstrate that Cernunnos-XLF has a major function in maintaining genomic stability.

Discussion

Our analyses of Cernunnos-XLF-mutant ES cells confirm that this protein functions as a basic NHEJ component. Like Cernunnos-XLF-mutant human fibroblasts (6, 7), Cernunnos-XLF mutant mouse ES cells are highly defective in the ability to support coding and RS joint formation in transient RAG-initiated V(D)J recombination assays. However, the level of coding and RS joins in Cernunnos-XLF-mutant ES cells, although very low, is higher than that observed in XRCC4-deficient ES cells. Moreover, unlike the very rare joins recovered from XRCC4-deficient ES cells, a large fraction of Cernunnos-XLF-mutant recovered joins appeared similar to those of WT. In this context, it is notable that there also is residual V(D)J recombination activity in the context of human Cernunnos-XLF mutations (6, 7). Notably, the level of residual RS join appears higher in human Cernunnos mutated fibroblast lines than we found in mouse ES cells (6, 7). However, it is unclear whether this represents a difference in the mutations, species, or tissues analyzed; in this context, DNA-PKc-deficient mouse ES cells have much higher levels of normal RS joints than the corresponding mouse fibroblast cells (19).

As for our Cernunnos-XLF-mutant mouse cells, residual coding and RS joins in human Cernunnos-XLF mutant fibroblast lines are composed of a mixture normal and abnormal joins. Thus, there either is a Cernunnos-XLF-independent means of generating some normal coding and RS joins, or most or all existing Cernunnos-XLF mutations are hypomorphic. With respect to our targeted Cernunnos-XLF mutation, the latter possibility implies production of very low levels of Cernunnos-XLF protein that retains basic NHEJ functions. In either case, assuming that Cernunnos-XLF does not affect the level of RAG cutting, the low level of recovered joins suggests that there should be many broken V, D, J, and RS ends that are not repaired normally in Cernunnos-XLF mutants. In this regard, a significant proportion of attempted plasmid-coding joins in NHEJ-deficient cells are not recovered by the bacterial drug selection assay because of large deletions that eliminate the Amp^R gene (25). Thus, the low recovery of coding and RS joins from Cernunnos-XLF mutant ES cells is consistent with the possibility that a significant proportion of coding joins from these cells also are not rejoined, joined with large deletions, or joined to other sequences in processes that could lead to translocations (see below).

Our findings have certain implications for potential Cernunnos-XLF functions. First, Cernunnos-XLF-mutant mouse ES cells are defective in both coding and RS joining, similar to mouse cells deficient for core NHEJ components (Ku, XRCC4, and Lig4) and clearly distinct from Artemis- or DNA-PKcs-deficient ES cells, which make nearly normal levels of RS joins. Furthermore, Cernunnos-XLF-mutant ES cells are highly radiosensitive, unlike DNA-PKcs or Artemis-deficient ES cells, which have little or no increase in radiosensitivity compared with WT cells (21). Thus, Cernunnos-XLF, like the other evolutionarily conserved NHEJ factors, is likely involved in most or all NHEJ reactions and not just the subset that requires end-processing. Also, Cernunnos-XLF-deficient ES cells, similar to XRCC4 and Lig4 deficient cells (26), but in contrast to DNA-PKcs and Artemis-deficient cells (21, 27), do not display high levels of telomere fusions. In the latter context, DNA-PKcs has been reported to have a telomere-capping function (27). It is not clear whether Cernunnos-XLF, XRCC4, and Lig4 lack a telomere capping function or whether such a function might be masked because of an additional requirement for these factors to mediate end-joining that leads to telomere fusions (28). Overall, our findings are consistent with Cernunnos-XLF's being part of an XRCC4/Lig4 complex and suggest that this protein might function by activating or enhancing the basic NHEJ ligation reaction (5, 10, 11).

We find that Cernunnos-XLF is required for efficient repair of DSBs generated by IR and for the maintenance of genomic stability under normal growth conditions, showing that Cernunnos-XLF, like other known NHEJ factors, functions as a genomic caretaker. Although the levels of spontaneous genomic instability in Cernunnos-XLF-deficient ES cells is lower than that of XRCC4-deficient ES cells, the distribution of the types of cytogenetic aberrations appears similar in these two mutants, consistent with a role for Cernunnos-XLF in the core NHEJ pathway. Genomic instability is a characteristic predisposing factor to tumorigenesis. In this context, deficiency for Ku70 and certain type of DNA-PKcs mutation can predispose to T cell lymphomas in mice (29–31). Moreover, deficiencies for any of the six previously characterized NHEJ factors, on a p53-deficient background, inevitably lead to the development of aggressive pro-B cell lymphomas with oncogenic translocations involving aberrant V(D)J recombination of the Ig heavy chain locus (1, 3). Our findings of genomic instability in Cernunnos-XLF-mutant mouse cells suggest that, like other NHEJ factors, Cernunnos-XLF may also function as a tumor suppressor, perhaps also by cooperating with checkpoint factors to suppress tumors that arise from aberrant V(D)J recombination.

Materials and Methods

Generation of Cernunnos-XLF-Deficient ES Cells. DNA sequences from the genomic Cernunnos-XLF locus were generated by PCR from TC1 ES cell DNA (129 strain). A targeting construct was designed to replace exons 4 and 5 with a Neo^R gene cassette oriented in the opposite transcriptional direction from the endogenous Cernunnos-XLF promoter. A 3.5-kb 3′ arm and 5.2-kb 5′ arm were PCR generated separately, cloned into pTOPO vector (Invitrogen, Carlsbad, CA), sequenced, and subcloned into pLNTK in the desired orientation. The targeting construct was then electroporated into TC1 ES cells, and successful targeting was assessed by Southern blot analyses using BamHI-digested genomic DNA and 3′/5′ genomic probes as outlined in detail in Fig. 1*A*. Four independent clones containing a targeted Cernunnos-XLF allele were obtained. Three were subjected to adenovirus-mediated Cre deletion to remove the Neo^R gene and then retargeted on their second Cernunnos-XLF allele. One clone was exposed to increased levels of G418 to select for homozygous mutant ES cells.

Northern Blot, RT-PCR, and Western Blot Analyses. Total RNA was isolated from WT (TC1), $Cer^{\Delta/\Delta}$, and $Cer^{N/\Delta}$ ES cell lines that were passaged at least twice without feeders by using TRIzol (Invitrogen). For Northern blot analyses, 20 μg of total RNA from each cell line was analyzed by standard Northern blotting procedures with a cDNA probe encoding the entire ORF of the murine *Cernunnos-XLF* gene. The full-length postsplicing transcript of murine *Cernunnos-XLF* is predicted to be 1.63 kb. Targeted deletion of exons 4 and 5 should reduce the transcript size to 1.43 kb. For RT-PCR analysis, cDNAs were made from total RNA isolated from individual ES clones by SuperScript II reverse transcriptase (Invitrogen). Primers flanking ORF of murine Cernunnos-XLF were used in the subsequent PCRs. In WT cells, the predicted product is ≈1.2 kb; after targeted deletion of exons 4 and 5, the predicted PCR product size is ≈1.0-kb. For Western blot analysis, 50 μg of total protein extract from WT (TC1), $Cer^{\Delta/\Delta}$, and $Cer^{N/\Delta}$ ES were subjected to SDS/PAGE and blotted with a rabbit polyclonal antibody against the C-terminal portion of Cernunnos-XLF [cat. no. A300–730A-1; Bethyl Laboratories (Montgomery, TX); Bethyl Laboratories report that the epitope recognized by this antibody maps to a region between residue 250 and the C terminus of human Cernunnos-XLF].

Radiation Sensitivity and DSB Repair Assays. Colony survival assays were performed as described (18, 21) to assess the radiation sensitivity of WT (TC1), $Cer^{\Delta/\Delta}$, $Cer^{N/\Delta}$, and $XRCC4^{-/-}$ ES cells. To measure DNA DSB repair after irradiation, 1×10^6 feeder-free ES cells were plated in each well of one six-well plate 12–18 h before irradiation. Immediately before irradiation, one well was harvested as an untreated control, and the rest of the wells were exposed to 80 Gy of radiation by using a ^{137}Cs source. The cells were harvested at various time points after irradiation as indicated, embedded in aragrose plugs, and analyzed by pulse-field gel electrophoresis as described (18). After running and before acquiring the image, the agarose plugs were cut out as a strip the same width as the thickness of the gel ("Well" in Fig. 2*B* and SI Fig. 4*C*) and turned 90° before drying along with the rest of the gel, to ensure a more uniform exposure of the well area. Three independent experiments were performed. Representative results are shown in Fig. 2*B*, and two additional experiments are shown in SI Fig. 1*C*.

Extrachromosomal V(D)J Recombination Assays. Transient V(D)J recombination assays were performed as described (20–22). V(D)J recombination efficiency was determined by the number of chloramphenicol–ampicillin double-resistant bacterial colonies versus the ampicillin-resistant colonies. The susceptibility to ApaLI digestion (which cleaves precise RS joins) of the chloramphenicol–ampicillin-resistant bacterial colonies was assayed to determine the fidelity of the RS joins. Selected chloramphenicol–ampicillin-resistant coding joint plasmids were isolated and sequenced.

Telomere-FISH Analysis. ES cells, not grown on feeders, were plated 24 h before the addition of colcemid (KaryoMAX Colcemid Solution; GIBCO, Carlsbad, CA) at 100 ng/ml for 1–2 h. ES cells were harvested by trypsinization, and metaphases were prepared as described (18, 21). T-FISH was performed as described (32). Briefly, telomeres are stained with a Cy3-labled $(CCCTAA)_3$ peptide nucleic acid probe (PNA; Applied-Biosystems, Foster City, CA), and DNA was counterstained with DAPI before mounting. Images were acquired through an Eclipse microscope (Nikon, East Rutherford, NJ) equipped with an interferometer (Applied Spectral Imaging, Migdal Ha'emek, Israel) and magnification ×40 and ×63 objectives. Chromosomal breaks were defined by loss of telomere signal from both sister chromatids. Such anomalies were unlikely to represent simple telomere loss for several reasons. First, in ≈50% of metaphases that have one or more chromosomes lacking telomere signals, a DAPI fragment containing the telomere signals and a DAPI-positive telomere-negative portion could be found, strongly suggesting that the lack of telomere signals resulted from a chromosome break rather than telomere erosion. Moreover, these small broken telomere-containing fragments do not contain centromeres and, therefore, could not be derived from broken dicentric chromosomes that might result from telomere fusions. In addition, in the many chromosomes that do not have anomalies, staining at the two telomeres appears normal, consistent with normal telomere length. Chromatid breaks were defined by loss of telomere signal from one of the two sister chromatids or a clearly broken DAPI signal in the middle of one chromatid. We cannot reliably score chromosomal gaps with the T-FISH assay; therefore, it is possible that the actual frequency of chromatid or chromosome breaks might be even higher than estimated. With T-FISH analysis, we could score only two kinds of translocations, specifically dicentric chromosomes and Robertsonian translocations. As we could not score translocations that did not disturb the centromere–telomere configuration of chromosomes, the actual level of translocations in Cernunnos-XLF-mutated cells may be higher than estimated.

We thank Dr. Sonia Franco for technical advice on cytogenetic analyses and critical review of this manuscript and Drs. Jean-Pierre de Villartay, Luigi Notarangelo, David Ferguson, and JoAnn Sekiguchi for critical review of this manuscript. This work was supported by National Institute of Health Grants AI35714 and CA92625 (to F.W.A.). F.W.A. is an investigator and G.L a postdoctoral associate of the Howard Hughes Medical Institute. S.Z. was supported by a fellowship from the Leukemia and Lymphoma Society of America.

1. Bassing CH, Alt FW (2004) *DNA Repair (Amsterdam)* 3:781–796.
2. Sonoda E, Hochegger H, Saberi A, Taniguchi Y, Takeda S (2006) *DNA Repair (Amsterdam)* 5:1021–1029.
3. Rooney S, Chaudhuri J, Alt FW (2004) *Immunol Rev* 200:115–131.
4. Ma Y, Pannicke U, Schwarz K, Lieber MR (2002) *Cell* 108:781–794.
5. Ahnesorg P, Smith P, Jackson SP (2006) *Cell* 124:301–313.
6. Buck D, Malivert L, de Chasseval R, Barraud A, Fondaneche MC, Sanal O, Plebani A, Stephan JL, Hufnagel M, le Deist F, *et al.* (2006) *Cell* 124:287–299.
7. Dai Y, Kysela B, Hanakahi LA, Manolis K, Riballo E, Stumm M, Harville TO, West SC, Oettinger MA, Jeggo PA (2003) *Proc Natl Acad Sci USA* 100:2462–2467.
8. Cantagrel V, Lossi AM, Lisgo S, Missirian C, Borges A, Philip N, Fernandez C, Cardoso C, Figarella-Branger D, Moncla A, *et al.* (2006) *Hum Mutat*, in press.
9. Moshous D, Callebaut, I., de Chasseval R, Corneo B, Cavazzana-Calvo M, le Deist F, Tezcan I, Sanal O, Bertrand Y, Philippe N, *et al.* (2001) *Cell* 105:177–186.
10. Callebaut I, Malivert L, Fischer A, Mornon JP, Revy P, de Villartay JP (2006) *J Biol Chem* 281:13857–13860.
11. Hentges P, Ahnesorg P, Pitcher RS, Bruce CK, Kysela B, Green AJ, Bianchi J, Wilson TE, Jackson SP, Doherty AJ (2006) *J Biol Chem* 281:37517–37526.
12. Frank-Vaillant M, Marcand S (2001) *Genes Dev* 15:3005–3012.
13. Kegel A, Sjostrand JO, Astrom SU (2001) *Curr Biol* 11:1611–1617.
14. Ooi SL, Shoemaker DD, Boeke JD (2001) *Science* 294:2552–2556.
15. Valencia M, Bentele M, Vaze MB, Herrmann G, Kraus E, Lee SE, Schar P, Haber JE (2001) *Nature* 414:666–669.
16. Teo SH, Jackson SP (2000) *Curr Biol* 10:165–168.
17. Celeste A, Petersen S, Romanienko PJ, Fernandez-Capetillo O, Chen HT, Sedelnikova OA, Reina-San-Martin B, Coppola V, Meffre E, Difilippantonio MJ, *et al.* (2002) *Science* 296:922–927.
18. Mostoslavsky R, Chua KF, Lombard DB, Pang WW, Fischer MR, Gellon L, Liu P, Mostoslavsky G, Franco S, Murphy MM, *et al.* (2006) *Cell* 124:315–329.
19. Gao Y, Chaudhuri J, Zhu C, Davidson L, Weaver DT, Alt FW (1998) *Immunity* 9:367–376.
20. Gu Y, Jin S, Gao Y, Weaver DT, Alt FW (1997) *Proc Natl Acad Sci USA* 94:8076–8081.
21. Rooney S, Alt FW, Lombard D, Whitlow S, Eckersdorff M, Fleming J, Fugmann S, Ferguson DO, Schatz DG, Sekiguchi J (2003) *J Exp Med* 197:553–565.
22. Hesse JE, Lieber MR, Gellert M, Mizuuchi K (1987) *Cell* 49:775–783.
23. Mills KD, Ferguson DO, Alt FW (2003) *Immunol Rev* 194:77–95.
24. Mills KD, Ferguson DO, Essers J, Eckersdorff M, Kanaar R, Alt FW (2004) *Genes Dev* 18:1283–1292.
25. Taccioli GE, Rathbun G, Oltz E, Stamato T, Jeggo PA, Alt FW (1993) *Science* 260:207–210.
26. d'Adda di Fagagna F, Hande MP, Tong WM, Roth D, Lansdorp PM, Wang ZQ, Jackson SP (2001) *Curr Biol* 11:1192–1196.
27. de Lange T (2002) *Oncogene* 21:532–540.
28. Smogorzewska A, Karlseder J, Holtgreve-Grez H, Jauch A, de LT (2002) *Curr Biol* 12:1635–1644.
29. Gu Y, Seidl KJ, Rathbun GA, Zhu C, Manis JP, van der SN, Davidson L, Cheng HL, Sekiguchi JM, Frank K, *et al.* (1997) *Immunity* 7:653–665.
30. Jhappan C, Morse HC, III, Fleischmann RD, Gottesman MM, Merlino G (1997) *Nat Genet* 17:483–486.
31. Li GC, Ouyang H, Li X, Nagasawa H, Little JB, Chen DJ, Ling CC, Fuks Z, Cordon-Cardo C (1998) *Mol Cell* 2:1–8.
32. Franco S, Gostissa M, Zha S, Lombard DB, Murphy MM, Zarrin AA, Yan C, Tepsuporn S, Morales JC, Adams MM, *et al.* (2006) *Mol Cell* 21:201–214.